A Highly Integrated Multi-Polarization Wideband Rectenna for Simultaneous Wireless Information and Power Transfer (SWIPT)

Chanfang Cao, Xuanming Zhang, Chaoyun Song, *Senior Member, IEEE*, Apostolos Georgiadis, *Fellow, IEEE*, and George Goussetis, *Senior Member, IEEE*

***Abstract*—Simultaneous wireless information and power transfer (SWIPT) presents a paradigm shift in future wireless sensing networks (WSNs) and industrial Internet of Things (IoT). A robust receiver capable of effectively capturing random signals from diverse environments is of utmost importance. To address this, we propose a multi-polarization wideband rectenna design, which integrates a novel symmetrical five-port hybrid-ring coupler and highly efficient Class-F rectifier in a compact manner. Due to the high symmetry between the ring coupler and the antenna, the impedance bandwidth (S_{11}<-10 dB) and the axial ratio bandwidth (AR< 3 dB) of the rectenna is highly coincident for different polarization methods, thereby effectively improving the operational stability and robustness of the multi-polarization rectenna. Our design has demonstrated over 46.3 % operational bandwidth (4.12-6.6 GHz) and over 10% circular polarization (CP) bandwidth. The wireless power receiving port has more than 55.6 % (up to 76.5 %) conversion efficiency over a power dynamic range of 0 - 10 dBm, while the optimal power routing of different ports can be obtained via the adjustment of the five-port coupler. Our wideband receiver excels in robust signal reception of arbitrary polarization waves, making it suitable for a range of real-world application scenarios in WSN and industrial IoT. It enables optimal power routing and efficient wireless powering, enhancing the overall performance of future wireless sensing networks and IoT applications.**

***Index Terms*—Information and power distribution, multi-polarization, rectenna, rectifiers, Simultaneous Wireless Information and Power Transfer.**

I. INTRODUCTION

WITH the explosion of 5G and wireless communication technologies, electromagnetic energy or radio frequency (RF) power over microwave (MW) bands has been widely distributed in domestic living environment [1].

Manuscript received February 23, 2023. *(Corresponding authors: Chaoyun Song)*

C. Cao is with the School of Information Engineering, Chang'an University, Xi'an 710064, China (e-mail: 2017224030@chd.edu.cn).

X. Zhang is with the School of Electronic Engineering, Xi'an University of Posts & Telecommunications, Xi'an 710121, China (e-mail: xuanmingzhang@xupt.edu.cn).

C. Song is with the Department of Engineering, King's College London, London, WC2R 2LS, UK (e-mail: chaoyun.song@kcl.ac.uk).

A. Georgiadis resides in 2582 CN The Hague, The Netherlands (e-mail: apostolos.georgiadis@ieee.org).

G. Goussetis is with the School of Engineering and Physical Sciences, Heriot-Watt University, Edinburgh EH14 4AS, Scotland, UK (g.goussetis@hw.ac.uk).

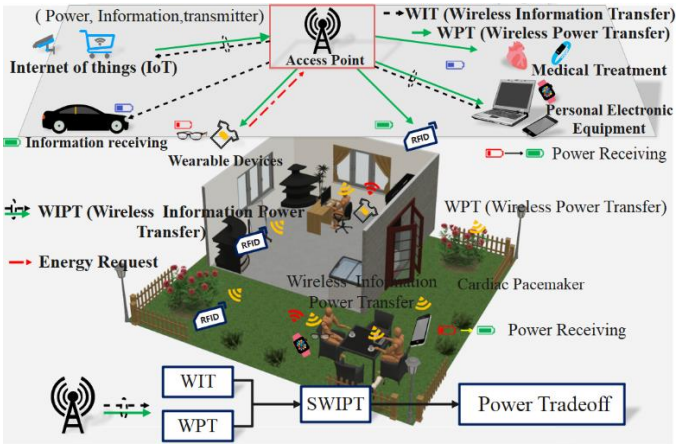

Fig. 1. SWIPT technology in industrial and commercial applications.

Academic and industrial activities are devoted to the harvesting of such energy, i.e. wireless power transfer (WPT) and environmental ambient energy harvesting (AEH) technologies, thereby becoming a research priority [2]-[4]. One of the key components is the rectenna, which is capable of converting the majority of RF energy into direct current (DC). More recently, emerging iterations between the IoT and artificial intelligence (AI) have facilitated the convergence of wireless communication and WPT technologies. A concept known as Simultaneous Wireless Information and Power Transfer (SWIPT) has been formulated [5]. The SWIPT could enable a continuous low-power way to provide energy for the terminal electronic devices using a battery-free fashion. The rectenna for SWIPT has been a key device to enable the integration of continuous access to power into the communication network of the Internet of Everything (IoE). Traditional ambient power density for radio communication is well below -40 dBm/cm^2. However, due to the development of 5G technology, the power density in space is rapidly increasing with a higher EIRP (e.g., 53 dBm for 5.8 GHz), which makes it gradually realistic to receive higher power (e.g., -10 dBm to 5 dBm) in certain locations and within reasonable distance from the base stations [4]. Further, the analysis of the tradeoff between received power and information is also of importance (see Fig. 1). For SWIPT application, the signal transmitter could radiate an increased power to dedicated location for an effective wireless charging purpose.

Conventional rectennas need the effective interconnection between antenna and rectifier to achieve RF to DC conversion for electromagnetic energy collection [6]-[11]. In order to

enable the function of wireless information and power transfer (WIPT), some researchers have used dual/multi-port antennas in combination with rectifying circuits [11], [12]. Further, all-polarized rectennas have also been implemented to be able to collect arbitrarily polarized waves as much as possible from the surrounding environment [13]. For single port rectennas, only one port can be combined with a rectifying circuit. For instance, the output port of the antenna needs to be switched for different purposes in time, which may cause delay slightly [9]. When the extra port is added, the rectenna not only collects energy but also receives information simultaneously. With the aid of a novel six-port coupler, the rectenna could eventually be able to collect the all-polarized wave [13]. Unwanted power loss due to polarization mismatch could be effectively reduced by switching among multi-polarizations [14]-[17]. Recently, some papers have realized the SWIPT by exploiting multi-port structures [18]-[21]. In [20], the ring antenna was connected to a 3dB hybrid coupler to switch between energy harvesting and information transmission at multi-polarizations, resulting in a narrower bandwidth of around 3.5% (5.77-5.98 GHz). However, the proposed rectenna is not available for polarization diversities when it was fixed to the rectifier. In particular, if the designed rectenna is operated in linear polarization (LP), both ports will be needed for rectifiers, therefore; it might not be possible to collect information and energy at the same time. In addition, the flexible distribution of the received information and power is difficult due to the limitations of the physical structure of the coupler [22].

The above analysis shows that traditional rectennas can only achieve energy collection, and the majority of rectennas applied to WIPT cannot achieve SWIPT. Although there are published rectennas for SWIPT applications, they still fail short to achieve all polarization of power and information transmission. At the same time, the robustness of the SWIPT rectennas is weak, which may make the application environment limited. Finally, there are also a few research that provides a detailed analysis of the power and information tradeoff received by SWIPT rectennas as well as the mitigation solutions.

In this paper, we present a novel all-polarization compact wideband high gain rectenna designed for SWIPT with a power tradeoff analysis. The main objective of the proposed rectenna is to achieve high-efficiency DC output within a defined range of medium power levels (10 dBm). A crucial aspect of our design is that the rectenna is co-designed as a whole unit, incorporating a CP antenna, hybrid coupler, and Class-F rectifier. By doing so, we overcome the operating frequency band limitations commonly found in conventional 50-ohm systems. The overall symmetry of our rectenna design is a key feature, which results in minimal frequency shifts in various indicators, including impedance bandwidth (IBW) and axial ratio bandwidth (ARBW), under left-hand circular polarization (LHCP), right-hand circular polarization (RHCP), and LP. This symmetry ensures the rectenna's stable and reliable operation, regardless of the polarization employed.

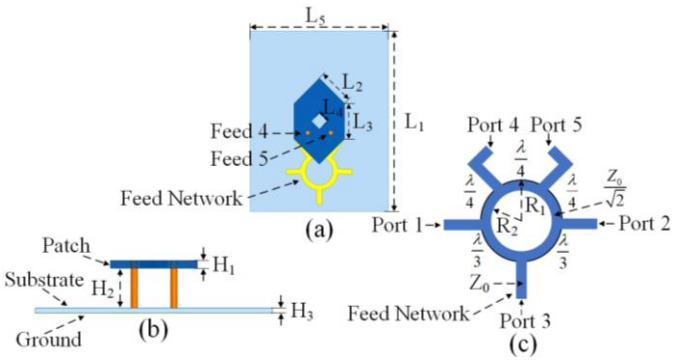

Fig. 2. Structure of multi-polarization high-gain wideband antenna. (a) Top view. (b) Side view. (c) Structure of the circuit hybrid ring. (L_1=75mm, L_2=22mm, L_3=5.8mm, L_4=4mm, L_5=70mm, H_1=1.2mm, H_2=6.5mm, H_3=0.78mm, R_1=6.76mm, R_2=4.84mm).

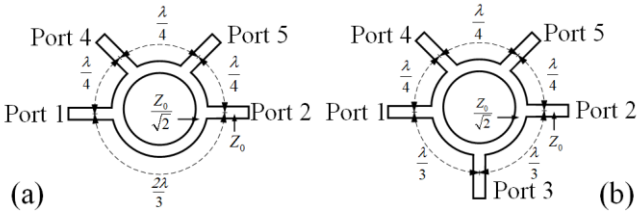

Fig. 3. Evolution of the hybrid-ring coupler geometry. (a) 4 ports and. (b) 5 ports hybrid-ring coupler.

By breaking the barriers of conventional 50-ohm systems and leveraging the advantages of our co-designed CP antenna, hybrid coupler, and Class-F rectifier, our proposed rectenna achieves exceptional performance in terms of wideband operation, high gain, and efficient power conversion. The results of our analysis demonstrate the rectenna's ability to deliver stable and reliable operation, making it a promising candidate for SWIPT applications that demand both high efficiency and wide bandwidth. Ultimately, the strongly robust receiver is advantageous in terms of structural/operational simplicity, all-polarized wave collection, and accurate distribution of power and information compared to the state-of-the-art receivers for SWIPT. The brief of the paper is organized as follows. Section II describes the structure of the all-polarized receiver antenna and provides a detailed discussion of the evolution of the symmetrical four-port ring coupler to a five-port structure. At the same time, we also show the basic model and structure of the rectifying circuit. Section III focuses on further improvements to the ring coupler, which can be varied in various ways to allow precise distribution of the power received by the antenna. Finally, Section IV gives a summary of the performance of the robustly designed receiver.

II. All-Polarization Rectenna Geometry and Design

The proposed rectenna consists of a square metal sheet on the upper layer, a circular five-port feed network on the lower layer and the high efficiency rectifying circuit. The receiving antenna is multi-polarized by controlling two ports on the feed network and one port integrated with the rectifying circuit.

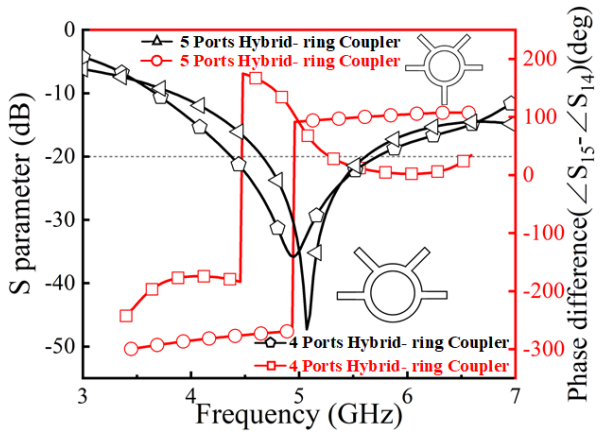

Fig. 4. Simulation of the S-parameters of a 4-port and 5-port hybrid-ring coupler and the phase difference between port 4 and 5 at a center frequency of 5 GHz.

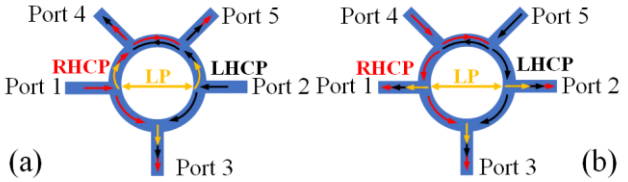

Fig. 5. Direction and distribution of signal/energy transfer for each port of the 5-port hybrid-ring coupler. (a) Distribution of energy and signal at the remaining three ports when port 1/2 is excited. (b) Distribution of energy/signal at the remaining three ports when Port 4 and Port 5 are excited.

A. Structure of Wideband Antenna

Fig. 2(a) demonstrates the designed antenna with three input/output ports, where the feed network is fabricated on a Rogers 4730 substrate (ε_r = 3.00, tan δ = 0.0028) with a thickness of 0.78 mm. The copper conductor length L_2 of the antenna has a significant effect on the operating frequency. When L_2 is chosen as 22mm, the center frequency of the antenna is 5 GHz. A slot of length L4 is cut in the center of the antenna to achieve better impedance matching. The theoretical center frequency (f_0) and parameters L_2, L_3, the following equations can be used.

$$f_0 = \frac{c}{2(L_2 + L_3)}\ (GHz) \qquad (1)$$

To guarantee the gain of the proposed antenna, the air layer used can effectively reduce the loss caused by the substrate, the height of the air layer (H_2) is shown in Fig. 2(b). Fig. 2(c) depicts the structure of the coupler in detail. Port 4 and port 5 are the antenna feed ports with a quarter wavelength distance between them. The ring coupler has a very symmetrical structure and when connected to the upper metal sheet, simultaneous or non-simultaneous excitation of the two ports (Port 1, Port 2) enables multi-polarization antenna [16]. The rectifying circuit is then combined with the last port (Port 3) to integrate the antenna with the rectifying circuit. This is followed by a discussion and analysis of the design of the feed network and the specific working mechanism.

The chosen 4-port hybrid-ring coupler has the advantages of easy impedance matching, a wider impedance bandwidth, and a smaller size for integration compared to conventional couplers [23]-[29]. As illustrated by (2) and (3), to achieve an

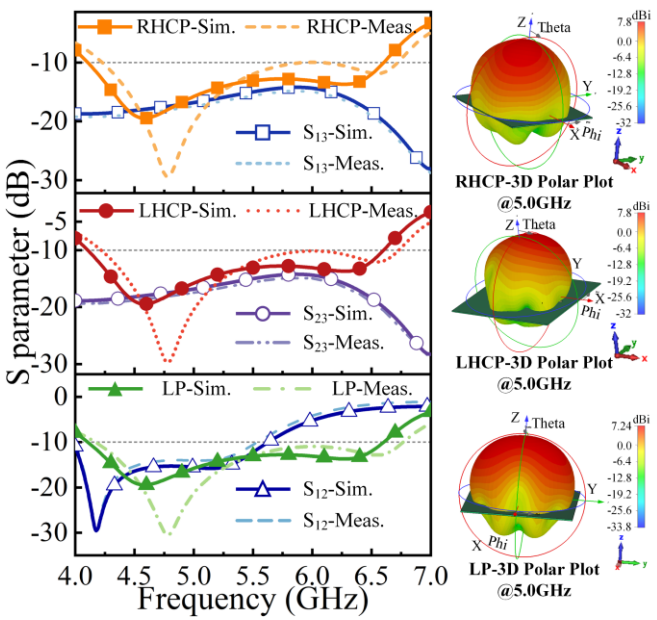

Fig. 6. Simulated and measured results of the S-parameters of the antenna in various operating modes (mode 1, mode 2). Plot of the gain and radiation direction of the antenna at the center frequency of 5 GHz.

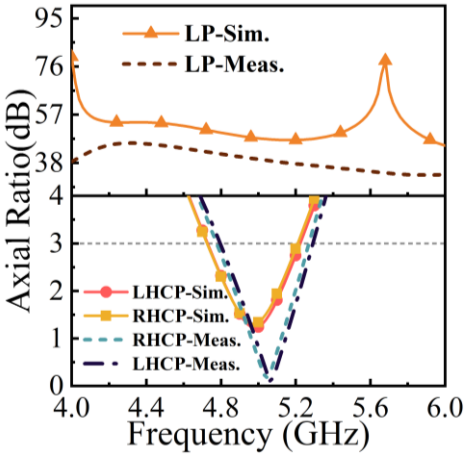

Fig. 7. Simulated and measured ARs at the two modes for CP and LP.

impedance value of 50 Ω for the input/output arm, the input impedance of the 4 ports hybrid-ring coupler can be calculated, where h, w, and ε_r means substrate's thickness, a width of the metal respectively, and relative permittivity.

$$Z_0 = \begin{cases} \frac{60}{\sqrt{\varepsilon_r}} In\left(\frac{8h}{w} + \frac{w}{4h}\right) & if\ w/h \le 1 \\ \frac{120\pi}{\sqrt{\varepsilon_{re}}[w/h + 1.39 + 0.67In(w/h + 1.44)]} \end{cases} \qquad (2)$$

$$\varepsilon_{re} = \frac{\varepsilon_r}{2} + \frac{\varepsilon_r - 1}{2}\left(1 + \frac{12h}{w}\right)^{-\frac{1}{2}} \qquad (3)$$

By adding a port to the 4 ports hybrid-ring coupler for connection to the rectifying circuit, the integration of the antenna with the rectifying circuit can be achieved, as well as the multi-polarization of the antenna (see Fig. 3). It also lays the foundation for SWIPT and the subsequent distribution of energy and information. Fig. 4 depicts the IBW (S_{11}<-20 dB)

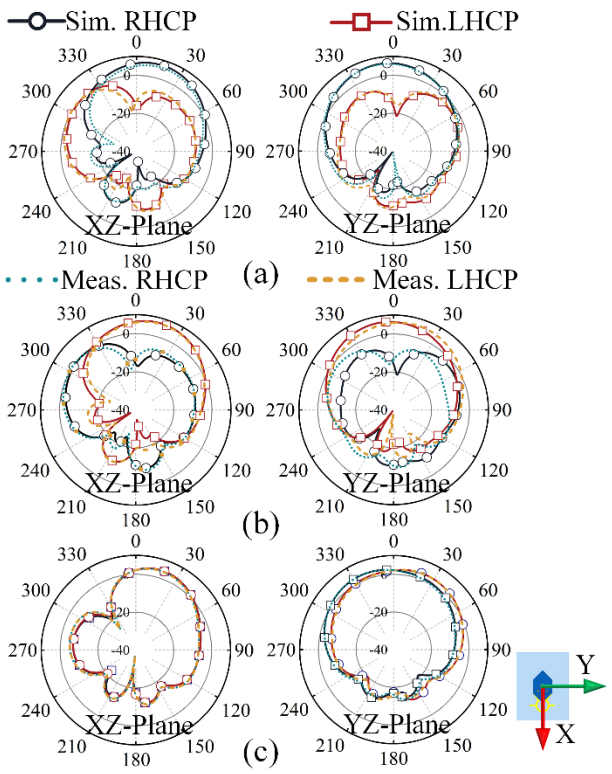

Fig. 8. Simulated and measured 2D radiation patterns of the designed antenna at 5GHz. (a) RHCP (b) LHCP (c) LP.

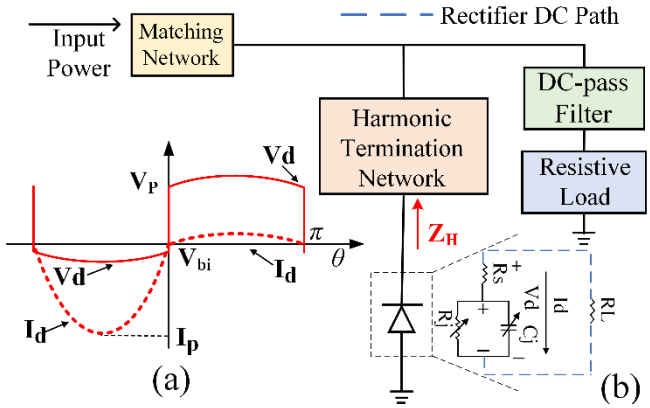

Fig. 9. (a) Medium input power at 10 dBm. (b)Basic topology of the Class-F rectifier.

Of the 4 ports hybrid-ring coupler is 26.9% (4.37 GHz-5.73 GHz) and the IBW (S_{11}<-20 dB) of the 5 ports hybrid-ring coupler is 20.6 % (4.54 GHz-5.58 GHz). It can also be observed that the phase difference when the 4/5 port hybrid-ring coupler are all fed by port 1 ($\angle S_{15}$ - $\angle S_{14}$) is 88°/92° at the center frequency of 5 GHz, close to the required 90° difference. The measured insertion loss of the coupler is less than XXX dB for all ports, thereby ensuring highly efficient power delivery from the antenna to rectifier.

The direction of signal (energy) transmission for each port of the 5-port hybrid-ring coupler is given in Fig. 5. In addition, due to the symmetrical construction of the hybrid-ring coupler, the output impedances are all close to 50 Ω and each port can be matched to the SMA connector. The proposed receiving antenna can operate in a variety of modes.

1) *Mode 1:* With one of the port (Port 1/Port 2) is excited and the other port (Port 2/Port 1) is connected matched load, the proposed antenna working in Mode 1. Fig. 5(a) and 5(b) show the difference in electrical length between port 4 and port 5 by a quarter of a wavelength (±90°), thus enabling the antenna to transmit/receive R/LHCP waves. Also, port 3 can recycle energy or signal from port 1/2 when the antenna is at the transmitting end. Thus, the R/LHCP antenna can be realized when port 1 or port 2 is excited alone.
2) *Mode 2:* With two ports (Port 1 and Port 2) are utilized in equal amplitude and the same phase to excite the antenna simultaneously, the currents of the two ports in opposite directions will be offset when passing through the circulator, and the remaining currents will reach port 4 and port 5 ports respectively. The antenna radiates electromagnetic waves for LP, named Mode 2. The designed feed network has simple requirements for the input signal, without controlling the antenna polarization by different phases, and a compact structure [20].

After simulation and measurement, S-parameters versus frequency are shown in Fig. 6. The proposed antenna of two modes is realized bandwidth (S_{11}<-10 dB) of 46.3% (4.12-6.6GHz) in the simulation. The IBW of the L/RHCP and LP antennas were measured to be 45.7% (4.22 -6.72 GHz), 45.3% (4.24 -6.72 GHz), and 47.2% (4.18 GHz-6.76 GHz) respectively. The measured results of the proposed antenna obtained are consistent with the computer simulation. The proposed rectenna is a remarkable integration that enables simultaneous transmission of information and power. It incorporates a three-port circular coupler and rectifying circuit into a single entity. The data provided pertains to the isolation between each input/output port and the rectifying circuit input port under three polarization modes. When we excite port 1 of the rectenna, it is polarized in RHCP. The isolation between output port 3 (connected to the rectifying circuit) and port 1 (S_{13} isolation) is depicted in Fig. 6. At the center frequency of 5 GHz, the value of S13 is -16.8 dB, and in the frequency band of 4.8-5.2 GHz, the isolation between port 1 and port 3 remains below -15 dB. Due to the antenna structure's symmetry, when port 2 is excited, indicating LHCP polarization, the isolation between port 2 and the rectifier circuit is similar to that observed in the RHCP mode. Furthermore, when both port 1 and port 2 are excited simultaneously, resulting in the rectenna being polarized in an LP manner, the isolation of both ports remains below -15 dB in the 4.8-5.2 GHz frequency band. These results underscore the fact that the power and information received by this rectenna experience minimal interference with each other. This enhanced isolation capability ensures efficient and reliable performance during simultaneous information and power transfer. Finally, the proposed antenna in both modes has a high gain, with values up to 7.8 dBi at the center frequency of 5 GHz.

The simulated and measured 3 dB AR bandwidths for L/RHCP antenna at θ = 0° are 10.3 % (4.72-5.23 GHz)/10%

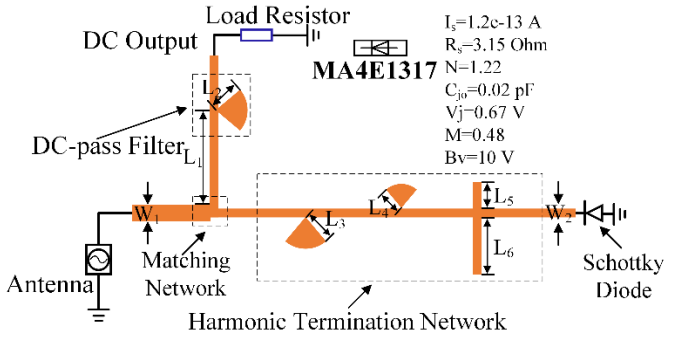

Fig. 10. Class-F low/high-power (0/10 dBm) rectifying circuit structure. (L_1=8.98mm, L_2=2.14mm, L_3=2.38mm, L_4=1.81mm, L_5=3.55mm, L_6=7.83mm, W_1=6.36mm, W_2=0.74mm).

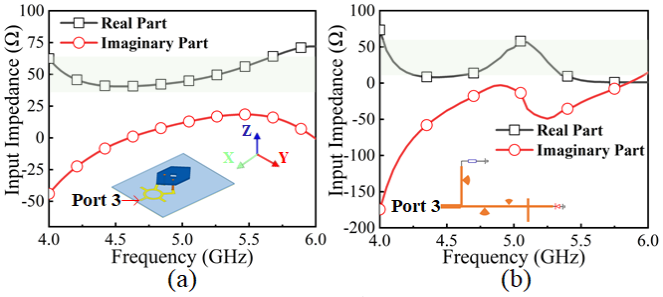

Fig. 11. Simulated (a) Input impedance of the designed receiving antenna. (b) Input impedance of the proposed rectifying circuit.

(4.72-5.22 GHz), and 9.9% (4.8-5.3 GHz)/ 9.8% (4.78-5.27 GHz), respectively (See Fig. 7). The AR at the center frequency of 5 GHz is 1.2 dB/1.3 dB (L/RHCP antenna). The above data proves that the ARBW coincides well with the L/RHCP of the antenna and that a wide ARBW can be achieved at the center frequency of 5 GHz. In addition, for the frequency range 4.7-5.2 GHz, the ARs are all greater than 30 dB for the LP antenna, verifying that the design allows the antenna to produce multi- polarization patterns.

To describe more clearly the polarization and radiation mode of the designed antenna, the radiation direction graph of the L/RHCP, and LP antenna was simulated and measured respectively, as shown in Fig. 8. The design coordinates of the antenna are also given. Fig. 8(a) confirms the radiation patterns of the designed antenna, at phi=0°, the cross-polarization of the proposed antenna is more than 21dB, and at phi=90°, the cross-polarization of the antenna is more than 22dB. When feeding port 1, the antenna can stably radiate RHCP, which is consistent with the results discussed above. Similarly, the cross-polarization of the antenna is more than 21 dB at phi=0°/90° (see Fig. 8(b)). This indicates that the proposed antenna stably radiates LHCP. At the same time, the implementation of a LP receiver antenna can also be demonstrated, as shown in Fig. 8(c).

In summary, the calculations and measurements of the S-parameters, ARs and radiation patterns demonstrate the designed antenna has good robustness and the performance indicators are in general agreement with the measured ones.

B. Medium Power Rectifying Circuit Design

To improve rectification efficiency, Class-F rectifiers draw on the design of high-efficiency non-linear power amplifiers [30]-[35]. High efficiency rectifying circuits are also an important part of the rectennas used for SWIPT. A model of the rectifying circuit connected to antenna port 3 is shown in Fig. 9. This Class-F rectifying circuit model consists mainly of resistive load, DC-pass filter, a matching network, and rectifying diode.

Typical single shunt topology includes the addition of a DC-pass filter before the load resistor, serving to filter out 1st, 2nd, and 3rd order energy. Additionally, a harmonic rejecting filter is placed before the rectifying circuit, not only to match the impedance of the diode and the antenna but also to suppress the 2nd and 3rd harmonics. It is worth noting that this approach to harmonic elimination may lead to significant insertion losses between the DC-pass filter and the harmonic termination network.

To address this issue and enhance the rectification efficiency of the diode while minimizing insertion losses, a modified single parallel structure is utilized (Fig. 9(b)). This new configuration involves placing the harmonic termination network, initially used for suppressing the 2nd and 3rd harmonics, before the diode. By doing so, the rectenna achieves improved performance and better rectification efficiency. This design alteration optimizes the harmonic rejection capabilities while reducing the losses introduced by the filters, resulting in a more efficient and effective rectifying circuit. The input impedance Z_H (f) at the harmonic termination network can be expressed as shown

$$Z_H(f) = 0, f = nf_1, n: even$$
$$Z_H(f) = \infty, f = nf_1, n: odd \quad (4)$$

When a nonlinear device, such as a diode, generates even order harmonics, it can be considered as a short termination, while odd harmonics result in an open termination. In practical design, suppressing the 3rd harmonic is often sufficient, and achieving this requires a harmonic termination network with two branches of different lengths to effectively suppress the 2nd and 3rd harmonics. By implementing this approach, the 2nd and 3rd harmonics produced by the diode are reflected back to the diode for re-rectification. As a result, these harmonics are practically eliminated at the pass-through filter, and the insertion loss associated with the harmonic termination network is significantly reduced [35]. This design strategy optimizes the harmonic rejection capabilities, resulting in a more efficient rectification process with minimized distortion and losses. It is a practical and effective way to achieve better performance in rectenna systems.

As technologies such as the Internet of Things and 5G continue to develop, there is a lot of microwave energy in people's daily lives. These energies are both low-power energy such as routers (WIFI) and radio frequency tags (RFID), and high-power energy such as base stations. Therefore, the rectifying circuit designed in this paper is capable of efficient rectification at a medium high power (10 dBm) and is of contemporary and future importance. The following is a detailed description of calculating the diode efficiency in the rectifier circuit at medium power (See Fig. 9 (a)).

TABLE I
SIMULATED INPUT IMPEDANCES

Receiving antenna		Rectifying circuit	
Freq.	Input impedance	Freq.	Input impedance
4.8 GHz	41.79+j*6.45 Ω	4.8 GHz	21.61−j*7.93 Ω
4.9 GHz	42.79+j*9.18 Ω	4.9 GHz	35.21−j*2.92 Ω
5.0 GHz	44.12+j*11.67 Ω	5.0 GHz	49.05−j*8.57 Ω
5.1 GHz	45.84+j*13.90 Ω	5.1 GHz	56.30−j*35.69 Ω
5.2 GHz	48.00+j*15.82 Ω	5.2 GHz	40.68−j*46.85 Ω

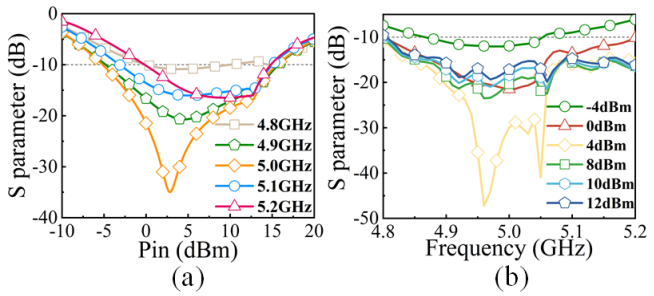

Fig. 12. Simulated S-parameters of the designed rectenna versus frequency. (a) The relationship between the five sampling frequencies and the S-parameters. (b) Variation of S-parameter values at different input powers.

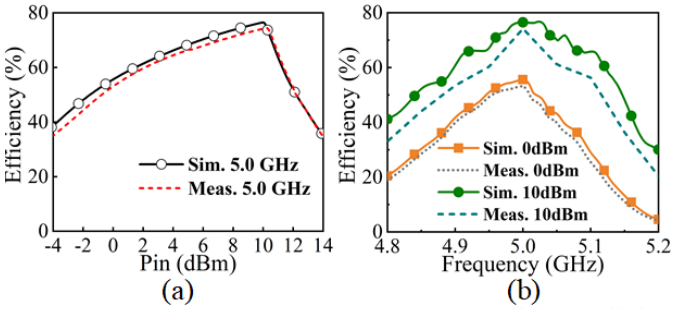

Fig. 13. Simulated and measured RF to DC conversion efficiency *Eff* of the proposed rectenna. (a) *Eff* versus input power at 5 GHz. (b) *Eff* versus frequency under the input power of 0 dBm and 10 dBm.

At medium input power, to predict the diode voltage (V_d) and current (I_d), the following equations can be used (5) and (6).

$$V_{d\_br} = \begin{cases} I_P R_S \sin(\theta) - V_{bi}, & -\pi < \theta < 0 \\ V_{br} + I_R R_S \sin(\theta) & 0 < \theta < \pi \end{cases} \quad (5)$$

$$I_{d\_br} = \begin{cases} I_P \sin(\theta), & -\pi < \theta < 0 \\ I_R \sin(\theta), & 0 < \theta < \pi \end{cases} \quad (6)$$

The P_{OUT} can be calculated by $P_{OUT} = 2(I_P - I_R)(-2I_P R_S + 2I_R R_S - \pi V_{bi} + \pi V_{br})$, the P_{LOSS,C_j} can be calculated by $P_{LOSS,C_j} = 22(I_P - I_R)(-2I_P R_S + 2I_R R_S - \pi V_{bi} + \pi V_{br})$, and the $P_{LOSS,R_S,V_{bi}}$ can be calculated by $P_{LOSS,R_S,V_{bi}} = \frac{16\pi^2 f^2 V_{br}^2 R_S C_j^2}{\alpha}$. The efficiency of the diode in the high input power case is expressed in (7) as follows:

$$\eta_{\_br} = \frac{P_{OUT}}{P_{OUT} + P_{LOSS,C_j} + P_{LOSS,R_s,V_{bi}}} \quad (7)$$

Next, the designed rectifying circuit is printed on Rogers 4730 with a thickness of H_3 = 0.78 mm in line with the designed receiving antenna substrate. The proposed Class-F rectifying circuit consists mainly of a matching structure, a fan-shaped filter, and a rectifier diode. This structure has the advantages of high rectification efficiency and compactness.

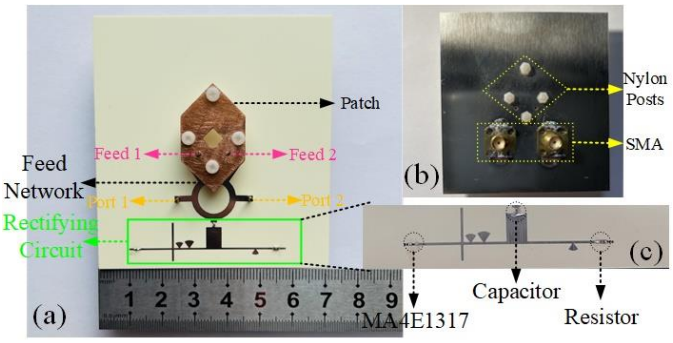

Fig. 14. Fabricated prototype of the designed rectenna. (a) Top view of multi-polarization wideband receiving rectenna. (b) Back view of the proposed rectenna. (c) The fabricated of Class-F rectifying circuit.

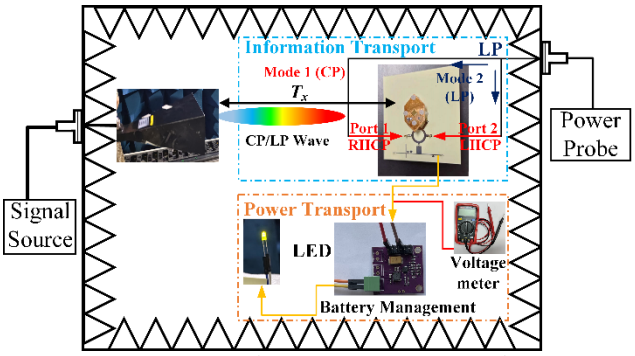

Fig. 15. The testing process for rectenna includes both information transfer and energy transfer. For accurate measurement results, the polarization of the transmission antenna needs to correspond to the receiving antenna. The test of energy transfer is indicated by a voltmeter connected to the battery management circuit at the output of the rectifying circuit.

Fig. 16. The ambient electromagnetic energy is supplied by a source at the left end, and at the right end an all polarization rectenna connected to an battery management module. The battery management module stabilizes the voltage value and light up the light emitting diode.

The core component in the rectifying circuit is the diode, which is used in this paper as model number MA4E1317. Some of the important parameters regarding the diodes have been listed, as shown in Fig. 10. To accurately represent the performance of the diode, a diode equivalent circuit model is used in this paper to improve the consistency of the diode with actual measurements [32]. As IoT and 5G technology continue to develop and spread, microwave energy in everyday life will also become increasingly complex and powerful [6]. The chosen MA4E1317 diode has a smaller series resistor (R_s)and a low zero-bias junction capacitance (C_{j0}) compared to other diodes, resulting in lower losses and higher efficiency. Its large reverse breakdown voltage (B_v) can be adapted to prevent breakdown at higher input powers.

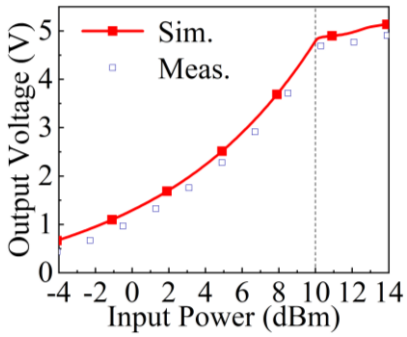

Fig. 17. Simulation and measurement of voltage versus input power variation at center frequency 5GHz.

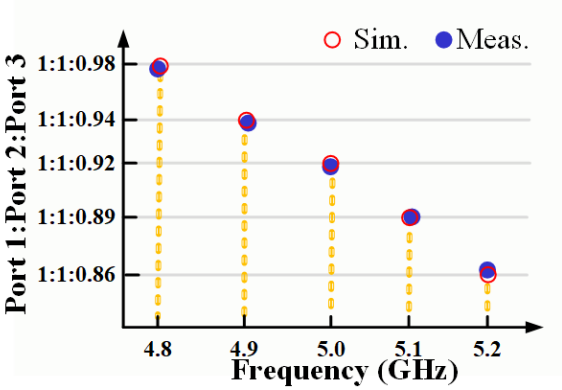

Fig. 18. Detailed simulation and measurement of the three-port (port 1, port 2, and port 3) power distribution under Case 1.

The RF-DC conversion efficiency (*Eff*) of a Class-F rectifying circuit is related to the output DC power (V_{out}), the input microwave power (P_{in}), and the carrier impedance (R_L) of the rectifying. In which, *Eff* can be expressed by

$$Eff = \frac{V_{OUT}^2}{R_L \cdot P_{in}} \times 100\% \quad (8)$$

Ultimately, the designed rectifying circuit is integrated with the multi-polarized antenna via port 3. The input impedance of the designed receive antenna port 3 and the input impedance of the rectifying circuit are shown in Fig. 11, respectively. Table I shows a comparison of the impedances between the proposed receiving antenna and the rectifying circuit at some important frequency points. The rectenna is co-simulated by using HFSS and ADS software [3]. The impedances of the proposed antenna are exported from port 3 and the resulting touchstone SNP file is imported into the ADS to describe the impedance variation of the proposed receiving antenna.

This method allows an approximate simulation of the designed antenna connected to the rectifying circuit. Conjugate matching enables the antenna to be matched to the rectifier circuit with a small matching loss. For example at a center frequency of 5 GHz the antenna port 3 impedance is 44.12 + 11.67j Ω and the rectifying circuit input impedance is 49.05 - 8.57j Ω. The widest ARBW of the proposed receiving antenna is 510 MHz (4.72-5.23 GHz), and the operating bandwidth of the rectifying circuit is 400 MHz (4.8-5.2 GHz), the IBW of the rectenna can reach 400MHz (4.8-5.2 GHz) under the co-simulation, which has a wide frequency band. It has also been confirmed that the rectenna works well in the low/high input power range involved (-4-14 dBm).

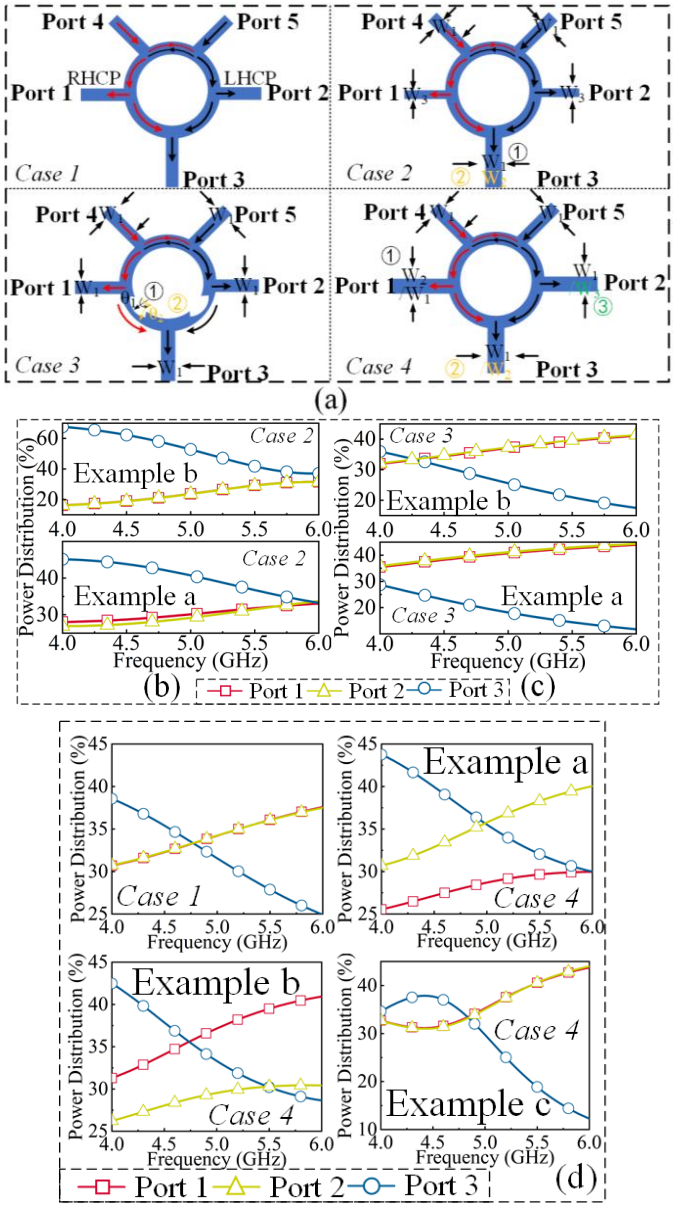

Fig. 19. The design options for the hybrid-ring coupler are broadly divided into four cases, each with a further detailed division according to structural characteristics. (a) Various structures of the 5 ports hybrid-ring coupler. Power distribution for (b) Case 2 and (c) Case 3. (d) Power distribution for case 1 and 4.

The input power range is -4 - 14 dBm, the range that can be used for both indoor collection (input ⩽ 0 dBm) of low power microwave energy such as WIFI, sensor networks, etc. to provide simultaneous reception of information and energy for indoor wireless electronics. It can also be used in external environments to collect energy from high-power (input ⩾ 10dBm) RF towers, and base stations.

Fig. 13 illustrates the variation of input power and sampling frequency points with respect to S-parameters, respectively. Fig. 12 (a) indicates that the S-parameter is less than -10 dB for all five sampling frequencies in the 0 dBm to 10 dBm input power interval. The rectenna is designed to operate between -5 dBm and 15 dBm when the center frequency is 5

TABLE II
PERFORMANCE COMPARISON OF PROPOSED DESIGN AND RELATED WORKS

References (year)	Frequency (GHz)		Operating Frequency Bandwidth	Polarization Mode	Flexible Power Distribution Methods	*Eff*	Integration and compactness of overall design	Size of rectenna (mm^2)
	Com.	MPT	Meas.					
[12] (2013)	6.1	5.8	<400MHz	LP	No (Different Frequency)	63 % @25 dBm 5.78 GHz	Average	(Two layers) 1.77λ×0.73λ @ 5.8GHz
[18] (2021)	0.83/2.4 (SWIPT)		NA	LP	No	63% @0.8μw/cm^2 2.4 GHz	Good	0.213λ×0.19λ×0.009λ @ 0.83GHz
[19] (2021)	2.4 (SWIPT)		NA	LP	No	74% @ 2dBm 2.4 GHz	Good	NA
[20] (2020)	5.8 (SWIPT)		LP:1.3% (5.75-5.83 GHz), LHCP:2.5% (5.7-5.85 GHz), RHCP:3.5% (5.77-5.98 GHz)	CP & LP	No	53.6% @0/0.5 dBm 5.8 GHz	Average	2.5λ×1.06λ @ 5.8GHz
[21] (2022)	2.4/5.8 (SWIPT)		LHCP:43 % RHCP:3.3 %	RHCP/ LHCP	NO	63% @ 12dBm 5.8 GHz	Average	2.6λ×2.6λ×0.077λ @ 0.83GHz
[22] (2022)	2.4 (WIPT/ SWIPT)		2.4GHz (Single point)	LP	Yes (Not precise enough)	60.7% @6dBm 2.4GHz	Poor	1.9λ×0.44λ@ 2.4GHz
This work (2023)	**5 (SWIPT)**		**LP: 47.2% (4.18-6.76 GHz), RHCP: 9.8% (4.78-5.27 GHz), LHCP: 9.9% (4.8-5.3 GHz)**	**True All Polarization**	**Yes (A definite proportion of power distribution)**	**53.1 % @0 dBm 5 GHz, 74.2 % @10 dBm 5 GHz**	**Excellent**	**1.25λ×1.17λ×0.1λ @ 5GHz**

GHz. The trend in Fig. 12(b) is consistent with Fig. 12(a), where the rectenna has a wide operating bandwidth while operating stably in the frequency range of 4.8-5.2 GHz.

The peak conversion efficiency (*Eff*) is reached when the input power is 10 dBm and the simulated/measured conversion efficiency of the rectenna is 76.5 %/74.2 % respectively (see Fig. 13). The simulated/measured efficiency of the rectenna is 55.6 %/53.1 % when the input power is 0 dBm. Please note the selected 0-10 dBm power range is an example to illustrate the effectiveness of rectifiers, the power range could be shifted to lower (e.g., -20 dBm) and higher (>15 dBm) values by exploiting alternative diodes like Skyworks SMS7630 and Infineon Technologies BAT-15 etc.

III. DISTRIBUTION OF INFORMATION AND POWER

A fabricated prototype of the proposed rectenna with a designed rectifying circuit is shown in Fig. 14. The rectenna is supported on two layers by four nylon posts with an air layer in between. The two ports of the feeder network (port 1, port 2) are soldered to 50Ω impedance SMA connectors, feed 1 and feed 2 are connected to the upper copper layer and the final port is used to integrate the rectifying circuit.

To illustrate more clearly what is involved in all-polarization rectenna testing, a measurement flow diagram has been drawn up as shown in Fig. 15. The measurements are divided into two main parts, i. e. the information transmission and power reception performance of the rectenna [36]. Test distance T_x of 1.0 m between the horn antenna as source and the multi-polarization receiver. Firstly, three types of polarized horn antenna are required as transmission antennas. When port 1/2 of the proposed antenna is excited, port 2/1 is connected matched load and the antenna can receive R/LHCP wave. Secondly, the antenna receives LP wave when given simultaneous, same phase, equal amplitude excitation at port 1 and port 2. Finally, port 3 is connected to the designed rectifying circuit and the battery management module is able to stabilize the voltage collected from the rectifying circuit to light up the LED.

In order to provide a clear demonstration of the proposed rectenna's energy harvesting capabilities in a real-world setting, we designed an experiment as illustrated in Fig. 16. In this experiment, a horn antenna with a bandwidth of 4-8 GHz (model W-0408LB15N) is used as the energy-emitting source. Positioned 1.0 meter away from the source is the designed all-polarized rectenna, which features a three-port ring coupler integrated with the rectifying circuit. It is important to note that port 1 and port 2, responsible for transmitting information, are connected to the broadband matching load beforehand. Port 3 is integrated with the rectifying circuit, and a battery management module is connected to the rectifying circuit's right end (at the load resistor) to stabilize the voltage output from the rectenna. To achieve voltage stabilization, we employ the BQ25504 DC-DC chip within the battery management module, which effectively stabilizes the voltage at approximately 3.0 V. The output port is connected to a light-emitting diode (LED), which emits a green light with a switch-on voltage of 3.0 V. The specific process of this setup involves the rectenna collecting energy from the environment, converting the RF energy into DC power through the rectifying circuit, and then stabilizing the voltage using the battery

management circuit. Finally, the stabilized voltage successfully illuminates the LED, demonstrating the successful energy harvesting capabilities of the rectenna. Overall, this experiment serves to showcase the efficient conversion and utilization of RF energy in a practical environment, highlighting the rectenna's effectiveness in energy harvesting applications.

Additionally, to demonstrate the effectiveness of wireless power and information reception of the proposed rectenna under various polarization states, we conducted experiments using in-house LHCP, RHCP, and LP transmitting antennas, all operating at a fixed EIRP of XX dBm (antenna gain + TX power). The proposed rectenna was utilized to receive signals at different polarizations. The results of these experiments, including the measured output DC voltage and RF power (measured using a spectrum analyzer), are presented in Fig. 17(a) and (b). The depicted graphs show that the proposed all-polarization rectenna successfully receives RF signals and generates rectified DC power simultaneously. Remarkably, the output DC power and received signal strength (RSS) remain virtually identical for LP, RHCP, and LHCP waves, all at the fixed EIRP. This noteworthy consistency in performance across different polarizations further validates the robustness and effectiveness of this novel rectenna design. These findings underscore the rectenna's capability to efficiently capture and convert RF energy while maintaining consistent reception quality across multiple polarization states. This successful demonstration emphasizes the rectenna's potential for practical applications in wireless power and information transmission scenarios.

Fig. 18 clearly demonstrates the rectenna structure of Case 1, with the power distribution of ports 1-3. After simulation and measurement, it can be observed that the percentage of energy received by the three ports is approximately equal. At present, many scholars have done more in-depth research on SWIPT, but few quantitative analyze has been done on the distribution of power and information received by rectenna [18]-[22].

In [20], The asymmetric feed structure used allows for unequal power distribution between two ports, but the asymmetry of the antenna structure may make the radiation direction uneven and thus affect the important performance of the rectenna. The proposed rectenna in this paper can freely and precisely distribute the output power of the three ports, i.e. the distribution of information and power, according to the requirements of use by transforming the structure of the hybrid-ring coupler (see Fig. 19). Fig. 20 depicts the variation of S-parameters versus frequency for a variety of cases (*Case 2-4*). The four distribution methods allow equal amounts of power to be output from the three ports (Case 1), or the power distribution can be adjusted by changing the width of the output ports (*Case 2*). It is also possible to adjust by means of a scalloped notch in the ring (*Case 3*), with similar results to (*Case 2*), without the need to re-match at the output port. However, the adjustment ratio may be lower compared to (*Case 2*). Finally, it is also possible to vary the output power (*Case 4*) by changing the width of one of the ports individually, and the three ports can obtain different amounts of power. The following four types of distribution are discussed and analyzed in detail.

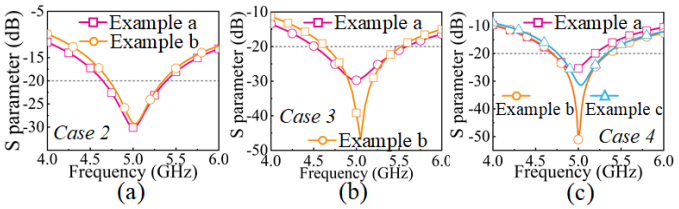

Fig. 20. Variation of S-parameters with frequency in (a) Case 2, (b) Case 3, (c) Case 4.

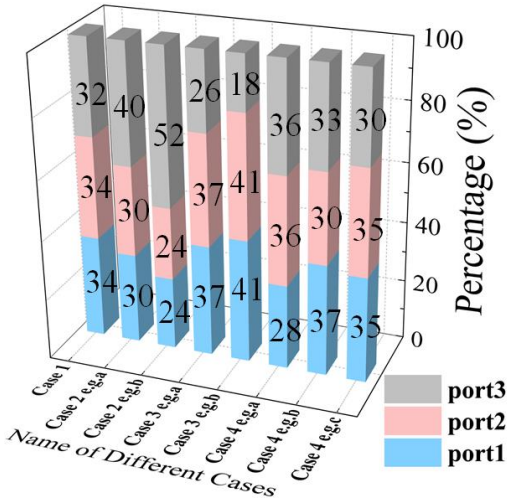

Fig. 21. Comparison of the normalized three-port power distribution of hybrid-ring coupler structures at a center frequency of 5 GHz.

1) *Case 1:* This example shows the hybrid-ring coupler used on the receiving antenna designed in Part I. This structure allows for an equal distribution of power. The width (W_1) of all ports of the hybrid-ring coupler is 1.88 mm in Fig. 19 (a). Fig. 4 establishes that the proposed coupler has an IBW (S_{11}<-20 dB) of 20.6% (4.54 GHz-5.58 GHz) and a center frequency of 5 GHz. This designed hybrid-ring coupler gives excitation at port 4 and port 5 to simulate the power received by the rectenna. The normalized output power ratio for the three ports is port 1: port 2: port 3 = 0.34:0.34:0.32. The lower power of port 3 compared to the other two ports may be due to some losses due to the distance on the ring coupler away from the output port. Overall the three ports receive almost equal power at 5GHz.
2) *Case 2:* The output power of the three-ports can also be adjusted by changing the width of port 1 and port 2. As in *example a*: the IBW (S_{11} < -20 dB) of the hybrid-ring coupler is 14.9 % (4.65 - 5.4 GHz) for port 1 and port 2 widths (W_3 = 0.6 mm, W_1 = 1.88 mm) in Fig. 20 (a). When the center frequency is 5GHz, the output power ratio of the three ports is port 1: port 2: port 3 = 0.3:0.3:0.4 (see Fig. 19 (b)). *Example b*: To further extend the output power of port, port 3 can also be achieved by increasing the width of port 3 (W_3 = 0.3 mm, W_1 = 2.7mm). Impedance bandwidth (S_{11}<-20 dB) is 13 % (4.7-5.36 GHz). The output power of the three ports at a frequency of 5 GHz is a ratio of port 1: port 2: port 3 = 0.24:0.24:0.52.
3) *Case 3:* The above solution (*Case 2*) is used to distribute power and information by changing the width of the

ports. The distribution of information and power can also be achieved by changing the in-ring impedance of the coupler. The advantage of this method is that it eliminates the need to add matching microstrip lines at port 1 and port 2. As in example a: when the angle of the sector slot is (θ_1 = 30°, R_1 = 7.2 mm), the IBW of the designed hybrid-ring coupler (S_{11} < -20 dB) is 23.8 % (4.45 - 5.65 GHz) ((see Fig. 20 (b))). The three output ports power ratio is port 1: port 2: port 3 = 0.37:0.37:0.26 at a center frequency of 5GHz (see Fig. 19(c)). For *example b*: When the angle of the sector slot is (θ_1 =45°, R_1=7.5mm), the IBW (S_{11}<-20 dB) of the coupler is 18.7% (4.6 - 5.55 GHz). The three output ports' power ratio is port 1: port 2: port 3 = 0.41:0.41:0.18.

4) *Case 4:* A change in power distribution can also be achieved by adjusting the width of one of the ports individually, as shown in Fig. 19(d). For *example a*: The IBW (S_{11}<-20 dB) of the proposed hybrid-ring coupler is 10.5% (4.68 - 5.2 GHz) for port1/2/3 with a port width of (W_2=1 mm) and port 2/1/2 and port 3/3/1 with (W_1=1.88 mm) (see Fig. 20 (c)). The three output ports power ratio is port 1: port 2: port 3 = 0.28:0.36:0.36 at a center frequency of 5GHz. Similarly, the normalized power distribution ratios for *example b* and *example c* are port 1：port 2：port 3=0.37:0.3:0.33 and port 1：port 2：port 3=0.35:0.35:0.3, respectively.

The above cases can be used to control the output power share by changing the proposed hybrid-ring coupler structure and selecting the applicable coupler for the application requirements. The individual hybrid-ring coupler configurations have corresponding advantages. For example, the hybrid-ring coupler structure in *Case 3* can be used directly without the need for an additional matching microstrip lines at the output port (port1 and port2). *Case 2*, however, enables a significant adjustment of the power distribution ratio. *Case 4* then allows for flexible adjustment of the power of the three ports so that they each have a different output power. Fig. 21 compares the power distribution percentages of the three ports at 5 GHz.

The performance comparison between the designed receiver and other rectennas for WIPT/SWIPT design is shown in Table II. It can be clearly observed that the our rectenna design has great advantages in bandwidth, gain and size. For example, the final achieved all-polarized rectenna has a relative bandwidth of 9.8%, which is an improvement of 7.5 times compared to the multi-polarized rectenna (with a relative bandwidth of 1.3%) [20]. The proposed design outperforms the state-of-the-art SWIPT rectennas in terms of overall integration and compactness. Importantly, our work innovatively uses a conjugate matching approach to integrate the antenna with the rectifying circuit [12] [18]-[22]. In addition, the rectification efficiency of the rectenna at input power 0/10 dBm is comparable to the state-of-the-art results. Most importantly, the rectenna proposed in this paper completely realizes the transmission of energy and information under all-polarization [12] [18] [20]-[22]. At the same time, the accurate proportion analysis and structure construction of energy and information have also been realized [20] [23]. Obviously, we have produced a robust receiver design that is suitable for real-time power supply and communication of terminal small electronic equipment under complex situations in the real world.

IV. Conclusion

A multi-port all-polarization compact wideband high-gain rectenna has been proposed for SWIPT applications. The proposed rectenna comprises a three-port hybrid-ring coupler and rectification circuitry, optimized for medium power reception (10 dBm). The rectenna's highly symmetrical structure, achieved by connecting a ring coupler via an annular square patch, not only facilitates multi-polarization (Circularly Polarized & Linearly Polarized), but also ensures a high level of performance robustness. Extensive simulations and measurements have been conducted, yielding results with excellent consistency. For the single-port feeding of LHCP and RHCP antennas, the impedance bandwidth (IBW) achieved was 45.7% (4.22-6.72 GHz) and 45.3% (4.24-6.72 GHz), respectively, with an axial ratio bandwidth (ARBW) of 9.8% (4.78-5.27 GHz) for both antennas. Moreover, the LP antenna, when operated with dual ports, demonstrated an impressive IBW of 47.2% (4.18-6.76 GHz). The use of ring couplers has provided significant advantages, and the experiments have been classified into four main categories (Case 1-4), each exhibiting its own unique characteristics. Within these categories, there are eight different structures, enabling accurate information and power distribution for practical scenarios.

As technology continues to advance, such as with 5G and IoT development, the microwave energy filling our living environments is expected to become more complex and random. In this context, the proposed rectenna's ability to handle a wide power range, maintain strong stability, and provide versatile power distribution is of great practical importance [37]. The innovative design and performance capabilities of this rectenna make it a promising candidate for SWIPT applications in various real-world scenarios, meeting the increasing demands of modern wireless technologies.

References

[1] C. Song et al., "Advances in Wirelessly Powered Backscatter Communications: From Antenna/RF Circuitry Design to Printed Flexible Electronics," *Proc. IEEE*, vol. 110, no. 1, pp. 171-192, Jan. 2022.

[2] Z. Zhang, H. Pang, A. Georgiadis and C. Cecati, "Wireless Power Transfer—An Overview," *IEEE Trans. Ind. Electron.*, vol. 66, no. 2, pp. 1044-1058, Feb. 2019.

[3] L. Li, X. Zhang, C. Song, W. Zhang, T. Jia and Y. Huang, "Compact Dual-Band, Wide-Angle, Polarization- Angle -Independent Rectifying Metasurface for Ambient Energy Harvesting and Wireless Power Transfer," *IEEE Trans. Microw. Theory Techn.*, vol. 69, no. 3, pp. 1518-1528, Mar. 2021.

[4] C. Song, P. Lu and S. Shen, "Highly Efficient Omnidirectional Integrated Multiband Wireless Energy Harvesters for Compact Sensor Nodes of Internet-of-Things," *IEEE Trans. Ind. Electron.*, vol. 68, no. 9, pp. 8128-8140, Sept. 2021.

[5] B. Clerckx, R. Zhang, R. Schober, D. W. K. Ng, D. I. Kim, and H. V. Poor, “Fundamentals of Wireless Information and Power Transfer: From RF Energy Harvester Models to Signal and System Designs,” *IEEE J. Sel. Areas Commun.*, vol. 37, no. 1, pp. 4-33, 2019.

[6] C. Song et al., "Matching Network Elimination in Broadband Rectennas for High-Efficiency Wireless Power Transfer and Energy Harvesting," *IEEE Trans. Ind. Electron.*, vol. 64, no. 5, pp. 3950-3961, May 2017.
[7] C. Liu, H. Lin, Z. He, and Z. Chen, "Compact patch rectennas without impedance matching network for wireless power transmission," *IEEE Trans. Microw. Theory Techn.*, vol. 70, no. 5, pp. 2882–2892, May 2022.
[8] C. K. Wang, B. J. Xiang, S. Y. Zheng, K. W. Leung, W. S. Chan and Y. A. Liu, "A Wireless Power Transmitter With Uniform Power Transfer Coverage," *IEEE Trans. Ind. Electron.*, vol. 68, no. 11, pp. 10709-10717, Nov. 2021.
[9] P. Lu and X. Yang, "Pattern Reconfigurable Rectenna With Omni-Directional/Directional Radiation Modes for MPT With Multiple Transmitting Antennas," *IEEE Microw. Wirel. Compon. Lett.*, vol. 29, no. 12, pp. 826-829, Dec. 2019.
[10] Naoki Shinohara, Ken Hatano, Tomohiro Seki, and Munenori Kawashima, "Development of Broadband Rectenna at 24GHz", *in 6th Global Symposium on Millimeter-Waves 2013 (GSMM2013)*, Sendai, 4.22-23, 2013.
[11] J. Bito, R. Bahr, J. G. Hester, S. A. Nauroze, A. Georgiadis and M. M. Tentzeris, "A Novel Solar and Electromagnetic Energy Harvesting System With a 3-D Printed Package for Energy Efficient Internet-of-Things Wireless Sensors," *IEEE Trans. Microw. Theory Techn.*, vol. 65, no. 5, pp. 1831-1842, May 2017.
[12] X.-X. Yang, C. Jiang, A. Z. Elsherbeni, F. Yang, and Y.-Q. Wang, "A novel compact printed rectenna for data communication systems," *IEEE Trans. Antennas Propag.*, vol. 61, no. 5, pp. 2532-2539, May 2013.
[13] S. F. Bo, J. -H. Ou, Y. Dong, S. -W. Dong and X. Y. Zhang, "All-Polarized Wideband Rectenna With Enhanced Efficiency Within Wide Input Power and Load Ranges," *IEEE Trans. Microw. Theory Techn.*, vol. 69, no. 7, pp. 7470-7480, Jul. 2022.
[14] A. Georgiadis and N. B. Carvalho, "A Convex Optimization Approach for the Design of Supergain Electrically Small Antenna and Rectenna Arrays Comprising Parasitic Reactively Loaded Elements," *IEEE Trans. Antennas Propag.*, vol. 70, no. 6, pp. 4674-4682, Jun. 2022.
[15] M. Li, R. Wang, H. Yao, and B. Wang, "A Low-Profile Wideband CP EndFire Magnetoelectric Antenna Using Dual-Mode Resonances," *IEEE Trans. Antennas Propag.*, vol. 67, no. 7, pp. 4445-4452, Jul. 2019.
[16] C. Cao, and C. Guo, "A Wideband High-Gain LHCP/RHCP Patch Antenna Based on Mirror Feed Method," *IEEE Antennas Wirel. Propag. Lett.*, vol. 21, no. 12, pp. 2317-2321, Dec. 2022.
[17] Q. Chen, J. Li, G. Yang, B. Cao, and Z. Zhang, "A Polarization Reconfigurable High-Gain Microstrip Antenna," *IEEE Trans. Antennas Propag.*, vol. 67, no. 5, pp. 3461-3466, May 2019.
[18] M. Wagih, G. S. Hilton, A. S. Weddell and S. Beeby, "Dual-Band Dual-Mode Textile Antenna/Rectenna for Simultaneous Wireless Information and Power Transfer (SWIPT)," *IEEE Trans. Antennas Propag.*, vol. 69, no. 10, pp. 6322-6332, Oct. 2021.
[19] M. Wagih, G. S. Hilton, A. S. Weddell and S. Beeby, "Dual-Polarized Wearable Antenna/Rectenna for Full-Duplex and MIMO Simultaneous Wireless Information and Power Transfer (SWIPT)," *IEEE Open J. Antennas Propag.*, vol. 2, pp. 844-857, 2021.
[20] P. Lu, C. Song and K. M. Huang, "A Two-Port Multipolarization Rectenna With Orthogonal Hybrid Coupler for Simultaneous Wireless Information and Power Transfer (SWIPT)," *IEEE Trans. Antennas Propag.*, vol. 68, no. 10, pp. 6893-6905, Oct. 2020.
[21] J. -H. Ou et al., "Highly-Isolated RF Power and Information Receiving System Based on Dual-Band Dual-Circular-Polarized Shared-Aperture Antenna," *IEEE Trans. Circuits Syst. I-Regul. Pap.*, vol. 69, no. 8, pp. 3093-3101, Aug. 2022.
[22] P. Lu, K. M. Huang, C. Song, Y. Ding and G. Goussetis, "Optimal Power Splitting of Wireless Information and Power Transmission using a Novel Dual-Channel Rectenna," *IEEE Trans. Antennas Propag.*, vol. 70, no. 3, pp. 1846-1856, Mar. 2022.
[23] Y.-K. Jung and B. Lee, "Dual-band circularly polarized microstrip RFID reader antenna using metamaterial branch-line coupler," *IEEE Trans. Antennas Propag.*, vol. 60, no. 2, pp. 786-791, Feb. 2012.
[24] H. Zhu and A. M. Abbosh, "A Compact Tunable Directional Coupler with Continuously Tuned Differential Phase," *IEEE Microw. Wirel. Compon. Lett.*, vol. 28, no. 1, pp. 19-21, Jan. 2018.
[25] H. -J. Yoon and B. -W. Min, "Two Section Wideband 90° Hybrid Coupler Using Parallel-Coupled Three-Line," *IEEE Microw. Wirel. Compon. Lett.*, vol. 27, no. 6, pp. 548-550, June 2017.
[26] W. Shi, Y. Yuan, S. S. Yang and B. S. Liang, "A modified broadband hybrid-ring directional coupler in W-band," *in Proc. 15th IEEE Conf. Electron. Packag. Technol. (ICEPT)*, 2014. pp. 1356-1358.
[27] Dong Il Kim and Gyu-Sik Yang, "Design of new hybrid-ring, directional coupler using lambda /8 or lambda /6 sections," *IEEE Trans. Microw. Theory Techn.*, vol. 39, no. 10, pp. 1779-1784, Oct. 1991.
[28] G. F. Mikucki and A. K. Agrawal, "A broad-band printed circuit hybrid ring power divider," *IEEE Trans. Microw. Theory Techn.*, vol. 37, no. 1, pp. 112-117, Jan. 1989.
[29] R. Haro-Baez, D. S. Benítez and D. Romero, "On the Design of a New 4x4 Coupler for C Band based on a 180° Coupler at Microstrip Technology," *in Proc. IEEE Colombian Conf. Commun. Comput. (COLCOM)*, 2019, pp. 1-6.
[30] X. Wang and A. Mortazawi, "Rectifier Array With Adaptive Power Distribution for Wide Dynamic Range RF-DC Conversion," *IEEE Trans. Microw. Theory Techn.*, vol. 67, no. 1, pp. 392-401, Jan. 2019.
[31] J. Guo, H. Zhang and X. Zhu, "Theoretical Analysis of RF-DC Conversion Efficiency for Class-F Rectifiers," *IEEE Trans. Microw. Theory Techn.*, vol. 62, no. 4, pp. 977-985, Apr. 2014.
[32] Q. Chen, X. Chen, H. Cai and F. Chen, "Schottky Diode Large-Signal Equivalent-Circuit Parameters Extraction for High-Efficiency Microwave Rectifying Circuit Design," *IEEE Trans. Circuits Syst. II-Express Briefs*, vol. 67, no. 11, pp. 2722-2726, Nov. 2020.
[33] S. Abbasian and T. Johnson, "Power-Efficiency Characteristics of Class-F and Inverse Class-F Synchronous Rectifiers," *IEEE Trans. Microw. Theory Techn.*, vol. 64, no. 12, pp. 4740-4751, Dec. 2016.
[34] F. Zhao, D. Inserra, G. Wen, J. Li and Y. Huang, "A High-Efficiency Inverse Class-F Microwave Rectifier for Wireless Power Transmission," *IEEE Microw. Wirel. Compon. Lett.*, vol. 29, no. 11, pp. 725-728, Nov. 2019.
[35] J. -h. Ou, S. Y. Zheng, A. S. Andrenko, Y. Li and H. -Z. Tan, "Novel Time-Domain Schottky Diode Modeling for Microwave Rectifier Designs," *IEEE Trans. Circuits Syst. I-Regul. Pap.*, vol. 65, no. 4, pp. 1234-1244, April 2018.
[36] S. Shen, J. Kim, C. Song and B. Clerckx, "Wireless Power Transfer With Distributed Antennas: System Design, Prototype, and Experiments," *IEEE Trans. Ind. Electron.*, vol. 68, no. 11, pp. 10868-10878, Nov. 2021.
[37] T. D. P. Perera, D. N. K. Jayakody, S. K. Sharma, S. Chatzinotas, and J. Li, "Simultaneous wireless information and power transfer (SWIPT): Recent advances and future challenges," *IEEE Commun. Surveys Tuts.*, vol. 20, no. 1, pp. 264-302, 2018.

Chanfang Cao was born in Shaanxi, China, in 1994. She received the M.Sc. degree in Information Engineering from Chang'an University, Xi'an, China, in 2020.

Her research interests include circularly polarized (CP) antenna and multi-polarization rectenna for wireless power transfer (WPT) and simultaneous wireless information and power transfer (SWIPT).

Xuanming Zhang received B.E. and Ph.D. degrees in electromagnetic fields and microwave technology from Xidian University, Xi'an, China, in 2014 and 2020, respectively.

He is currently a Lecturer with the School of Electronic Engineering, Xi'an University of Posts & Telecommunications. His research interests include metasurfaces design, wireless energy harvesting, and simultaneous wireless information and power transfer (SWIPT).

Chaoyun Song (Senior Member, IEEE) received BEng. MSc and PhD degrees in electrical engineering and electronics from The University of Liverpool (UoL), Liverpool, UK, in 2012, 2013 and 2017, respectively.

He is currently an Associate Professor (Senior Lecturer) with the Department of Engineering, King's College London, London, UK. Prior to this, he was an Assistant Professor with the School of Engineering and Physical Sciences (EPS), Heriot-Watt University, Edinburgh, Scotland, UK. He has published more than 100 papers (including 39 IEEE transactions) in peer-reviewed journals and conference proceedings. His current research interests include wireless energy harvesting and power transfer, rectifying antennas (rectennas), flexible and stretchable electronics, metamaterials and meta-surface, and low-power sensors.

Dr. Song was the recipient of many international awards such as the IEEE AP-S Young Professional Ambassador 2023. He won the BAE Systems Chairman's Award in 2017 for the innovation of next generation global navigation satellite system antennas. In 2018, Dr Song has been session chairs and/or TPC members for EuCAP2018, IEEE AP-S Symposium 2021, IEEE VTC2022-fall, EuCAP2023, has been a Guest Editor for Wireless Communications and Mobile Computing and is an Associate Editor for Frontiers in Communications and Networks.

Apostolos Georgiadis (Fellow, IEEE) received the Ph.D. degree in electrical engineering from the University of Massachusetts, Amherst, MA, USA.,He has held positions as a System Engineer within industry in the USA and as a Senior Researcher and a Group Leader in microwave subsystems in Spain. From 2016 to 2017, he was an Associate Professor with Heriot-Watt University, Edinburgh, U.K. He is currently a Patent Examiner with the European Patent Office. He has authored more than 200 articles in peer-reviewed journals and international conferences. His current research interests include energy harvesting and wireless power transfer, RFID technology, active antennas, and inkjet and 3-D printed electronics.,Dr. Georgiadis was a Fulbright Fellow and an EU Marie Curie Global Fellow. His research has received several Best Paper Awards and the 2016 Bell Labs Prize. He was an Associate Editor of IET Microwaves Antennas and Propagation and IEEE Microwave and Wireless Components Letters. He co-founded and was an Editor-in-Chief of Wireless Power Transfer. He was a Distinguished Lecturer of the IEEE Council on RFID. He is a URSI Fellow and the 2017-2020 Chair of the URSI Commission D.

George Goussetis (Senior Member, IEEE) received the Diploma degree in electrical and computer engineering from the National Technical University of Athens, Greece, in 1998, B.Sc. degree in physics (First Class) from University College London, U.K., in 2002, and the Ph.D. degree from the University of Westminster, London, U.K., in 2002.,In 1998, he joined the Space Engineering, Rome, Italy, as a RF Engineer and in 1999 the Wireless Communications Research Group, University of Westminster, U.K., as a Research Assistant. From 2002 to 2006, he was a Senior Research Fellow with Loughborough University, U.K. He was a Lecturer (Assistant Professor) with Heriot-Watt University, Edinburgh, U.K., from 2006 to 2009, and a Reader (Associate Professor) with Queen's University Belfast, U.K., from 2009 to 2013. In 2013, he joined Heriot-Watt as a Reader and was promoted to a Professor in 2014, where he currently directs the Institute of Sensors Signals and Systems. He has authored or coauthored over 500 peer-reviewed papers five book chapters one book and four patents. His research interests are in the area of microwave and antenna components and subsystems.,Dr. Goussetis has held a research fellowship from the Onassis foundation in 2001, a research fellowship from the U.K. Royal Academy of Engineering from 2006 to 2011 and European Marie-Curie experienced researcher fellowships in 2011 and 2012 and again in 2014 and 2017. He is the co-recipient of the 2011 European Space Agency Young Engineer of the Year Prize, the 2011 EuCAP Best Student Paper Prize, the 2012 EuCAP Best Antenna Theory Paper Prize, and the 2016 Bell Labs Prize. He has served as an Associate Editor for IEEE Antennas and Wireless Propagation Letters.